



CHORUS

This is the accepted manuscript made available via CHORUS. The article has been published as:

Spectroscopy of ^{28}Na : Shell evolution toward the drip line

A. Lepailleur *et al.*

Phys. Rev. C **92**, 054309 — Published 16 November 2015

DOI: [10.1103/PhysRevC.92.054309](https://doi.org/10.1103/PhysRevC.92.054309)

Spectroscopy of ^{28}Na : shell evolution towards the drip line

A. Lepailleur,¹ K. Wimmer,^{2,3,4} A. Mutschler,⁵ O. Sorlin,¹ J.C. Thomas,¹ V. Bader,⁶ C. Bancroft,³ D. Barofsky,³ B. Bastin,¹ T. Baugher,⁶ D. Bazin,⁶ V. Bildstein,⁷ C. Borcea,⁸ R. Borcea,⁸ B. A. Brown,⁶ L. Caceres,¹ A. Gade,⁶ L. Gaudefroy,⁹ S. Grévy,¹⁰ G. F. Grinyer,¹ H. Iwasaki,⁶ E. Khan,⁵ T. Kröll,¹¹ C. Langer,⁴ A. Lemasson,^{1,6} O. Llidoo,¹ J. Lloyd,³ E. Lunderberg,⁶ F. Negoita,⁸ F. de Oliveira Santos,¹ G. Perdikakis,^{3,4} F. Recchia,⁶ T. Redpath,³ T. Roger,¹ F. Rotaru,⁸ S. Saenz,³ M.-G. Saint-Laurent,¹ D. Smalley,⁴ D. Soehler,¹² M. Stanoiu,⁸ S. R. Stroberg,⁶ M. Vandebrouck,⁵ D. Weisshaar,⁶ and A. Westerberg³

¹Grand Accélérateur National d'Ions Lourds (GANIL),

CEA/DSM - CNRS/IN2P3, B. P. 55027, F-14076 Caen Cedex 5, France

²Department of Physics, The University of Tokyo, Hongo, Bunkyo-ku, Tokyo 113-0033, Japan

³Department of Physics, Central Michigan University, Mt. Pleasant, Michigan 48859, USA

⁴National Superconducting Cyclotron Laboratory, Michigan State University, East Lansing, Michigan 48824, USA

⁵Institut de Physique Nucléaire, IN2P3-CNRS, F-91406 Orsay Cedex, France

⁶Department of Physics and Astronomy and National Superconducting Cyclotron Laboratory, Michigan State University, East Lansing, Michigan, 48824-1321, USA

⁷Department of Physics, University of Guelph, Guelph, ON N1G 2W1, Canada

⁸IFIN-HH, P. O. Box MG-6, 76900 Bucharest-Magurele, Romania

⁹CEA, DAM, DIF, F-91297 Arpajon, France

¹⁰Centre d'Études Nucléaires de Bordeaux Gradignan-UMR 5797, CNRS/IN2P3,

Université de Bordeaux 1, Chemin du Solarium, BP 120, 33175 Gradignan, France

¹¹Institut für Kernphysik, Technische Universität Darmstadt, 64289 Darmstadt, Germany

¹²Institute of Nuclear Research of the Hungarian Academy for Sciences, P.O. Box 51, Debrecen, H-4001, Hungary

Excited states in ^{28}Na have been studied using the β -decay of implanted ^{28}Ne ions at GANIL/LISE as well as the in-beam γ -ray spectroscopy at the NSCL/S800 facility. New states of positive ($J^\pi=3^+, 4^+$) and negative ($J^\pi=1^-, 5^-$) parity are proposed. The former arise from the coupling between $0d_{5/2}$ protons and $0d_{3/2}$ neutron, while the latter are due to couplings of $0d_{5/2}$ protons with $1p_{3/2}$ or $0f_{7/2}$ neutrons. While the relative energies between the $J^\pi=1^+-4^+$ states are well reproduced with the USDA interaction in the $N=17$ isotones, a progressive shift in the ground state binding energy (by about 500 keV) is observed between ^{26}F and ^{30}Al . This points to a possible change in the proton-neutron $0d_{5/2}$ - $0d_{3/2}$ effective interaction when moving from stability to the drip line. The presence of $J^\pi=1^--4^-$ negative parity states around 1.5 MeV as well as of a candidate for a $J^\pi=5^-$ state around 2.5 MeV give further support to the collapse of the $N=20$ gap and to the inversion between the neutron $0f_{7/2}$ and $1p_{3/2}$ levels below $Z=12$. These features are discussed in the framework of Shell Model and Energy Density Functional calculations, leading to predicted negative parity states in the low energy spectra of the ^{26}F and ^{25}O nuclei.

PACS numbers: 21.60.Cs, 23.20.Lv, 27.30.+t

I. INTRODUCTION

The first disappearance of a magic shell was proposed more than 30 years ago for the neutron magic number $N=20$. This discovery arose from the combined works on atomic masses [1], nuclear radii [2] and nuclear spectra [3, 4] of nuclei around ^{32}Mg . This discovery was later confirmed by complementary measurements of the reduced transition probability values $B(E2; 0^+ \rightarrow 2^+)$ [5], of the quadrupole and magnetic moments [6], of the neutron knock-out cross sections [7], as well as of the evolution of the energies and configurations of 0_2^+ states between ^{34}Si [8] and ^{32}Mg [9]. This list is not exhaustive and complementary information can be found in Ref.[10]. Theoretically, the works of Refs [11–13] described this onset of collectivity at $N=20$ as due to the combination of a shell gap reduction and the excitations of particles from the normally occupied orbital to the first orbital of the upper shell. These excitations lead to a significant increase of

correlations, eventually bringing the *intruder* configuration from the upper shell energetically below the normal configuration. The nuclei for which the ordering of the intruder and normal configurations is inverted belong to the so-called 'Island of Inversion' [13].

The shell evolution of neutron orbits as a function of the proton number is illustrated in Fig. 1 for the $N=20$ isotones. This figure has been elaborated with the monopole proton-neutron interactions obtained in the shell model approach of Ref. [14] that match the few experimental observations made at that time. At $Z=8$, the neutron $0d_{3/2}$, $1p_{3/2}$ and $0f_{7/2}$ orbits are unbound, the $N=20$ gap is weaker than the $N=16$ gap, and the ordering of the $1p_{3/2}$ and $0f_{7/2}$ orbits is reversed compared to what is observed in the valley of stability. While filling the proton $0d_{5/2}$ orbit from $Z=8$ (^{28}O) to $Z=14$ (^{34}Si), the $N=20$ gap increases as the $N=16$ gap is reduced. After $Z=14$, the filling of the $1s_{1/2}$ and $0d_{3/2}$ proton orbits keeps the $N=20$ gap unchanged between $Z=14$ and $Z=20$. The formation of the $N=20$ shell gap, as well as

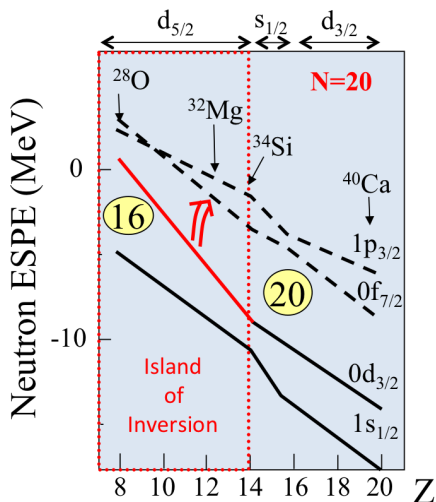


FIG. 1: (color on line) Neutron effective single-particle energies (ESPE) of the $N=20$ isotones between $Z=8$ and $Z=20$ based on the work of Ref.[14]. The slope of the lines corresponds to the strength of the proton-neutron monopole interactions. The red line, which has the largest slope, shows the effect of the strong $d_{5/2}$ - $d_{3/2}$ proton-neutron monopole interaction when the proton $d_{5/2}$ is filled.

the inversion between the neutron $0f_{7/2}$ and $1p_{3/2}$ orbitals are profound structural changes in the shells that are likely caused by the hierarchy between the proton-neutron monopole interactions involved: the $0d_{5/2}$ - $0d_{3/2}$ interaction is much larger than the others involved such as the $0d_{5/2}$ - $0f_{7/2}$ and $0d_{5/2}$ - $1p_{3/2}$ ones, as described in Refs. [14–16]. When the neutron $1p_{3/2}$ orbit becomes unbound, a further reduction of the monopole interactions involving this low- l orbital may be present.

The $0d_{5/2}$ - $1p_{3/2}$ and $0d_{5/2}$ - $0f_{7/2}$ proton-neutron monopole interactions are so far poorly constrained by experimental data, and the constancy of the $0d_{5/2}$ - $0d_{3/2}$ proton-neutron interaction from the valley of stability to the drip-line has not been tested so far. To achieve these goals, the evolution of the $0d_{3/2}$, $1p_{3/2}$ and $0f_{7/2}$ neutron single-particle energies should be determined from the Si to O isotones.

However, the $N=20$ nuclei lying in the island of inversion are deformed already in their ground state. Consequently, their configurations are strongly mixed; the single particle strength corresponding to each neutron orbital is expected to be fragmented over several states. Extracting the spherical energy centroid from many, weakly populated, levels is experimentally challenging. A further difficulty arises from the fact that the $N=20$ nuclei with $Z=10$ and $Z=8$ are weakly bound or unbound. They are difficult to produce in experiments and their study would often require the treatment of the continuum. In order to study these interactions and their behavior towards the neutron drip line, we take advantage of the fact that large $N=14$ and $N=16$ shell gaps are present around $Z=8$ -10 [17–23], where the $N=20$ gap is weakened. The $N=17$

nuclei can therefore be described mainly with a single neutron in the $d_{3/2}$, $p_{3/2}$ or $f_{7/2}$ orbit, without a large mixing with neighboring shells.

Recent experimental observations [24–27] have brought remarkable credit to the theoretical description of Fig. 1 around $(N=16, Z=8)$, suggesting an inversion between the neutron $1p_{3/2}$ and $0f_{7/2}$ orbits in the $N=15$ and $N=17$ Ne isotopes. These experiments have also demonstrated that the $N=20$ gap is small. In addition, the works of [21–23] have proven that the $N=16$ shell gap is large at $Z=8$, while Ref. [28] suggests that the $N=16$ gap somehow persists at $Z=10$ in ^{26}Ne , as witnessed by its vibrational behavior.

The best way to extract information about the aforementioned monopole *and* multipole parts of the nuclear interaction is therefore to study odd-odd nuclei in the $N=17$ isotones. The coupling of protons and neutrons in the $d_{5/2}$ and $d_{3/2}$ orbits will lead to $J^\pi=(1-4)^+$ states in the $^{30}_{13}\text{Al}_{17}$, $^{28}_{11}\text{Na}_{17}$ and $^{26}_9\text{F}_{17}$ isotones that span from near stability to the neutron drip line. In a similar manner, the coupling of the protons in the $d_{5/2}$ orbit with neutrons in the $1p_{3/2}$ ($0f_{7/2}$) orbit leads to $J^\pi=(1-4)^-$ ($J^\pi=(1-6)^-$) negative parity states in the same nuclei. However such studies are tedious as several experimental methods are often required to produce all the states of these multiplets for nuclei that are not so easily produced at radioactive ion beam facilities. The first $J=1-4$ positive parity states in ^{30}Al have been obtained recently using the Gammasphere array [29]. The negative parity states proposed from 2.29 MeV [29, 30] on are assumed to originate from the neutron $f_{7/2}$ orbital. In ^{26}F three different experimental techniques were required to study the bound $J^\pi=2^+, 4^+$ states [28, 31] and the unbound $J^\pi=3^+$ state [32]. So far there is no evidence of negative parity states in ^{26}F below the neutron emission threshold of 1.070(62) MeV [28]. As for the ^{28}Na nucleus, there are only candidates for the $J^\pi = 1_1^+$ and $J^\pi = 2_1^+$ states that were deduced from a previous β -decay study of ^{28}Ne [33]. The present study aims at determining the energy of the missing $J^\pi = 3_1^+$ and $J^\pi = 4_1^+$ states and providing information on the presence of negative parity states in ^{28}Na to confirm the lowering of the neutron $1p_{3/2}$ and $0f_{7/2}$ orbits toward $Z=8$. To achieve these goals two complementary experimental techniques were required. We first repeated the β -decay experiment of ^{28}Ne at the GANIL/LISE facility with a larger statistics as compared to [33] and we secondly used the in-beam spectroscopy technique at the NSCL/MSU facility to detect the γ -rays of ^{28}Na in the GRETINA Ge detector array [34] produced in the neutron and proton removal reactions from $^{31,32}\text{Mg}$.

II. β -DECAY EXPERIMENT

A. Experimental technique

The ^{28}Ne nuclei were produced at the GANIL facility through the fragmentation of a 77.6 MeV/u ^{36}S beam with an intensity of $7 \cdot 10^{11}$ pps on a 237 mg/cm^2 Be target. Nuclei of interest were selected by the first magnetic dipole of the LISE [35] spectrometer. Moreover, a wedge-shaped Be degrader was placed at the intermediate dispersive focal plane of the spectrometer to induce an additional selection between the nuclei transmitted after the first magnetic selection. The magnetic field of the second dipole was tuned to match the energy losses of the nuclei of interest, while others were rejected. The shape of the degrader was designed to preserve the achromatism of the beam line, i.e. ions with central trajectories are slowed down by $1066 \mu\text{m}$ of beryllium while those having a higher (lower) velocity traverse a thicker (thinner) layer of degrader. The selected nuclei were identified from their energy losses in a stack of three $500 \mu\text{m}$ Si detectors (labeled as $\Delta E_{i=1-3}$ in the upper part of Fig. 2) and from their time-of-flight referenced to the cyclotron radio frequency. The spectrometer set-up was optimized for ^{26}F , but as shown in the lower part of Fig. 2, a fraction of the ^{28}Ne ions was also transmitted at a rate of 10 pps, corresponding to 22% of the implanted nuclei. A total of 3.24×10^6 ^{28}Ne nuclei were implanted in a 1 mm-thick double-sided Si stripped detector (DSSSD) composed of 256 pixels (16 strips in both the X and Y directions) of $3 \times 3 \text{ mm}^2$ located at the final focus of LISE. β -particles were detected in the same strip of the DSSSD as the precursor nucleus ^{28}Ne . The depth of implantation was controlled using an Al degrader that could be tilted with respect to the beam axis. A Si(Li) detector of 5 mm thickness was placed downstream of the DSSSD to ensure that the ^{28}Ne ions were properly implanted and not just passing through it, as well as to discriminate very light particles in the beam that pass through the telescopes and give rise to fake signals in the Ge detector at zero degree. The mean energy-loss of β particles arising from the decay of nuclei implanted in the middle of the DSSSD is of about 200 keV. This energy becomes significantly smaller when the nucleus is implanted close to an edge of the detector and the β particle is emitted in the direction of this edge. With a spread in implantation depth of more than $200 \mu\text{m}$ in this relatively thin DSSSD a large fraction of β particles deposit energies that are close to the electronic threshold. This explains that a rather low detection efficiency of about 60% is achieved, as discussed below. The β energy threshold in each strip of the DSSSD was obtained by using the energy spectrum of the β -particles detected in the DSSSD as well as in the thicker Si(Li) detector. Indeed, by applying this coincidence requirement, the background signals in the DSSSD is suppressed and the true β energy threshold can be clearly determined.

Four Ge detectors of the EXOGAM array [36] sur-

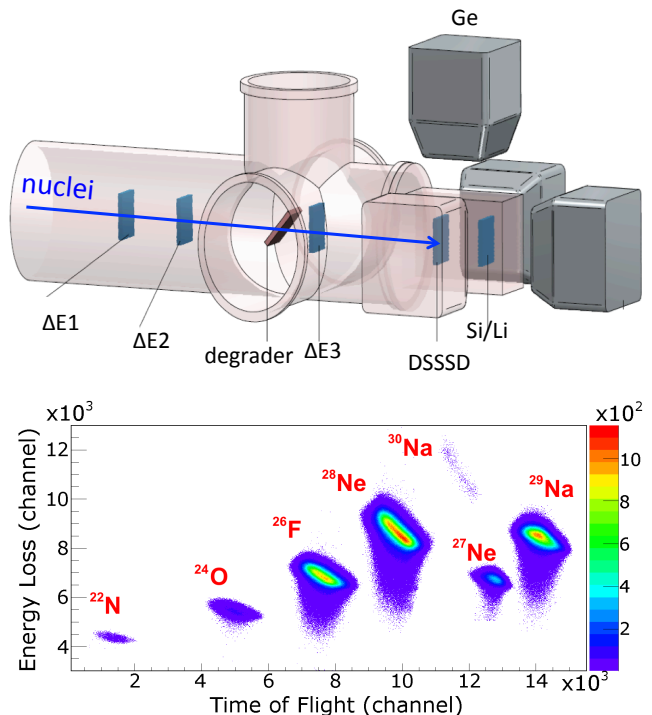


FIG. 2: (color on line) Top: Schematic view of the experimental set-up for the study of the β -decay of ^{28}Ne . Bottom: Identification of the nuclei produced in the experiment and implanted in the DSSSD through their energy loss and time of flight. The color code indicates the number of identified ions.

rounded the DSSSD to detect the γ -rays following the β -decay of implanted nuclei. γ -ray efficiencies of 6.5(3)% at 1 MeV and 4.2(3)% at 3.2 MeV were determined using calibrated γ -ray sources as well as known decay branches from the ^{27}Ne , $^{29,30}\text{Na}$ nuclei also implanted in the same setup (Fig. 2). A total β -efficiency of 60(1)% was determined from the comparison of the intensity of a given γ -ray belonging to the decay of ^{28}Ne gated or not on a β -ray.

B. Beta-decay scheme of ^{28}Ne

Fig. 3 displays the γ -ray energy spectrum obtained with a β -particle correlated in space and time up to 40 ms (top) and between 120 and 1000 ms (bottom) after the implantation of a ^{28}Ne precursor. Owing to the short lifetime of ^{28}Ne (see below), the transitions from Fig. 3 belonging to its β -decay are more intense in the upper spectrum, while those caused by daughter decays or other implanted nuclei are dominating the bottom spectrum. Consistent half-lives of $T_{1/2}=18.2(5)$ ms and $18.6(2)$ ms are found from the β -decay time spectrum of ^{28}Ne gated on the 863 keV and 2063 keV transitions seen in Fig. 3, respectively. These values are also in accordance with $T_{1/2}(^{28}\text{Ne}) = 18.4(5)$ ms derived in Ref. [33].

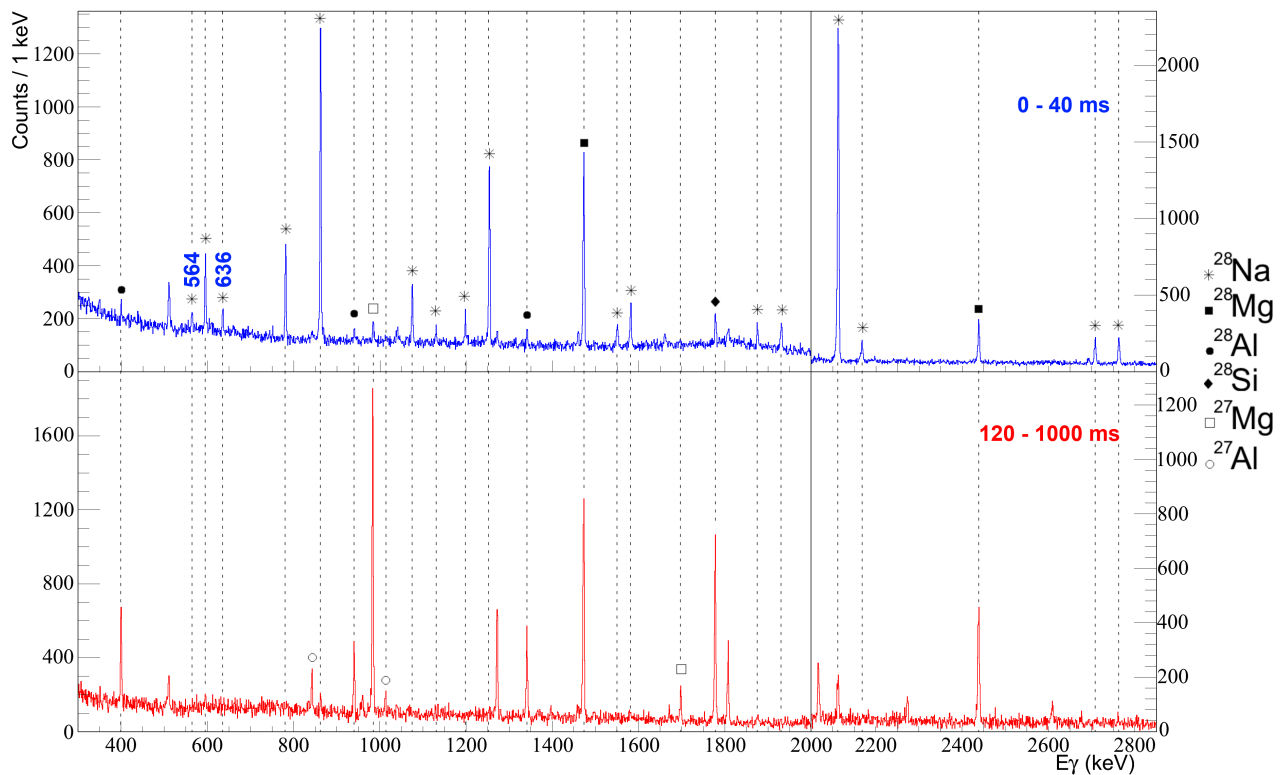


FIG. 3: (color on line): β -gated γ -ray spectra obtained up to 40 ms (upper spectrum) and between 120 ms and 1000 ms (bottom spectrum) after the implantation of a ^{28}Ne nucleus. Identified γ -rays are shown with different symbols. The new ones at 564(1) and 636(1) keV attributed to the decay of ^{28}Ne are visible on the left hand side of the top spectrum. Above 2 MeV the scale of the y axis of the spectrum changes, the number of counts should be read from the scale on the right.

The level scheme shown in the left part of Fig. 10 is established from β -gated γ - γ coincidences following the implantation of a ^{28}Ne nucleus. Based on their direct β -decay feeding from the 0^+ ground state of ^{28}Ne and Gamow-Teller β -decay selection rules, we propose a $J^\pi=1^+$ spin parity value for the states at 2714, 2118 keV and for the ground state of ^{28}Na . The β feedings to the ^{28}Na ground state as well as to unbound states (leading to the β -delayed neutron emission) are derived from the intensities of the observed lines seen in Fig. 3 populating excited states in the ^{28}Mg and ^{27}Mg nuclei from the decays of ^{28}Na and ^{27}Na studied in Refs. [37, 38]. The present β feedings in the decay of ^{28}Ne agree with those determined in Ref. [33] for most of the states, including the unbound states. For comparison β feedings have been calculated in the shell model using the USDA interaction [40], the results are shown on the right in Fig. 10. As for the β -decay of ^{26}Ne [39], the feeding of only three of the four predicted 1^+ states is observed in the β -decay of ^{28}Ne below the neutron separation energy.

With the exception of the 3286 keV and 3512 keV γ lines, all the transitions belonging to the ^{28}Ne decay to ^{28}Na proposed in [33] are observed here and listed in Table I. Assuming β feedings of 1.3(3) and 0.9(2)% for the 3286 keV and 3512 keV excited states, respectively, as given in Ref. [33], a γ efficiency of about 4% at 3.2 to

TABLE I: List of states (ranked by increasing energies), spin assignments J^π , energies of the final state and corresponding γ -ray transitions E_γ , absolute intensities I_γ^{abs} (normalized to 100 ^{28}Ne decays) and β feedings I_β observed in the β -decay of ^{28}Ne to ^{28}Na .

E_i (keV)	J^π	E_f (keV)	E_γ (keV)	I_γ^{abs} (%)	I_β (%)
0	1^+	0	0		55(7)
55.2(5) ^a	2^+	0	55		< 2 ^a
691(1)	(3^+)	55	636(1)	0.3(1)	< 0.1
1131(1)	(3^+)	0	1131(1)	0.2(1)	< 0.5
		55	1076(1)	1.0(1)	
1255(1)	(2^+)	0	1255(1)	2.7(2)	< 0.4
		55	1200(1)	0.5(1)	
		691	564(1)	0.3(1)	
1932(1)	(2^+)	0	1932(1)	0.5(1)	< 0.2
		55	1877(2)	0.4(1)	
2118(1)	1^+	0	2118(2)	0.8(1)	18(1)
		55	2063(1)	14.2(12)	
		55	863(1)	3.6(3)	
2714(1)	1^+	0	2714(2)	0.9(1)	4.2(2)
		55	2659(1)	0.9(1)	
		1131	1583(1)	0.7(1)	
		1932	782(1)	1.1(1)	
		2118	596(1)	0.6(1)	

^ataken from Ref. [33]

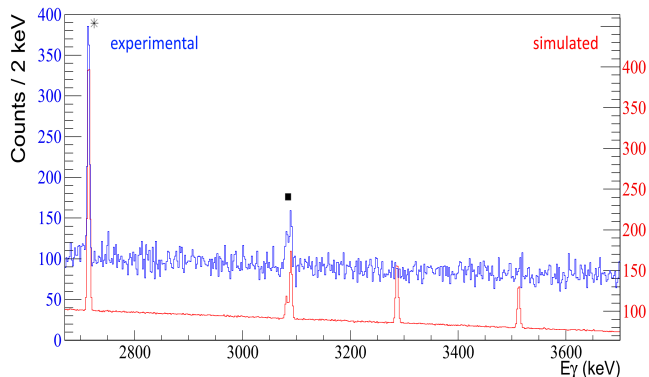


FIG. 4: (color on line) Experimental (top, blue) and simulated (bottom, red) β -gated γ -ray spectrum between 2.7 and 3.7 MeV for a time window of 40 ms. The γ line at 2714 keV is observed from the present experiment with a total intensity of 0.9%. The doublet of states of 3082 and 3087 keV, whose respective branching ratios of 1.3(3) and 4.0(6)% were determined in Ref. [?], originates from the decay of ^{28}Na to ^{28}Mg . The simulation reproduces remarkably well the amplitude of the three experimental peaks as well as the background contribution using measured feeding intensities and decay branching ratios. It also shows how many counts would have been observed if the levels at 3286 keV and 3512 keV (and their corresponding γ transitions) were existing with β feedings of 3σ weaker than the values of 1.3(3) and 0.9(2)%, respectively, proposed in Ref. [33].

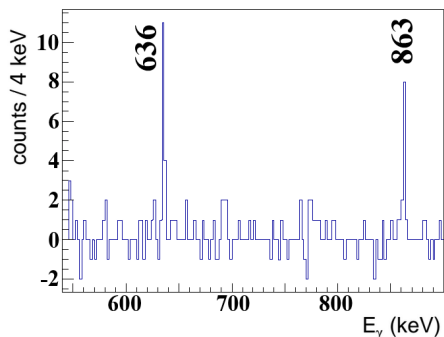


FIG. 5: β -gated γ -ray spectrum in coincidence with the 564(1) keV transition.

3.5 MeV from our work, and a time window of 40 ms between the implantation of ^{28}Ne nuclei and its β decay events, these transitions should have been seen with about 500 counts in each γ peak if present. The simulation of Fig. 4 shows the expected γ spectrum obtained if the branching ratios for these transitions were 3σ weaker than the proposed values. As the peaks at 3286 keV and 3512 keV are not observed in our experiment, we can conclude that they probably do not belong to the ^{28}Ne decay scheme. As the spatial correlation information between implanted nuclei and β -decay events was not used in Ref. [33], it is possible that these γ rays were wrongly assigned to the ^{28}Ne decay.

We observe two new γ rays at 564(1) keV and

636(1) keV of similar weak intensities in Fig. 3 that are in mutual coincidence (see Fig. 5) as well as in coincidence with the 863(1) keV γ rays de-exciting the 2118(1) keV level in ^{28}Na . The summed energy of these two γ transitions, 1200(2) keV, matches the energy of the 1200(1) keV transition coming from the decay of the 1255(1) keV state to the state at 55.2(5) keV in ^{28}Na . We therefore propose a new level in ^{28}Na , the placement of which (691(2) keV) was derived using the information obtained in the second experiment described below.

To propose spin parity assignments to the identified states shown in Fig. 10 and listed in Table I, the following strategy is adopted. We start with the assumption that the ground state of ^{28}Ne has $J^\pi=0^+$ and all levels that are directly fed in the β -decay (ground state, 2118 and 2714 keV excited states) are assigned to $J^\pi=1^+$ as the associated $\log ft$ values (4.15(6), 4.24(3) and 4.75(3)) match allowed Gamow-Teller transitions. These $J^\pi=1^+$ levels likely decay to states in ^{28}Na following the property that $M1$ are usually strongly dominating over $E2$ transitions for similar γ decay energies. Furthermore, when needed, we use the comparison to shell model predictions using the USDA interaction [40] as a guidance to propose spin assignments to the observed levels. This interaction, derived from the fit of more than 600 states in 77 nuclei in the sd shell, leads to a root mean square deviation of only 170 keV for all considered states, suggesting that the comparison to data is fairly reliable.

As stated above, the ground state of ^{28}Na has $J^\pi=1^+$. The excited state at 55 keV is likely to have $J^\pi=0,2^+$ as a larger spin difference between this state and the ground state would have resulted in a longer-lived 55 keV isomeric transition, in contradiction with the value of 1.4(4) ns found in the in-beam study of ^{28}Na described in the next section. Between the $J^\pi=0,2^+$ candidates, the $J^\pi=2^+$ value seems the most reasonable, considering that the USDA prediction gives the first 2^+ state at 182 keV and the first 0^+ state at a much higher energy of about 2 MeV.

Based on the existence of a predicted $J^\pi=3^+$ state at similar energy, the absence of feeding from the upper $J^\pi=1^+_{2,3}$ states and its exclusive decay branch to the 55 keV level rather than to the ground state, the state at 691 keV is a good candidate for having $J^\pi=3^+$. Indeed a $J^\pi=3^+$ state mainly decays through an $M1$ transition to the $J^\pi=2^+$ at 55 keV with a γ -ray of 636 keV rather than through an $E2$ transition to the $J^\pi=1^+$ ground state. The same arguments are used to propose a spin parity assignment $J^\pi=3^+$ to the state at 1131 keV, which decays dominantly (by a factor of 9) to the $J^\pi=2^+$ at 55 keV rather than to the $J^\pi=1^+$ ground state.

We propose a spin parity assignment $J^\pi=2^+$ to the state at 1255 keV since it is strongly fed from the $J^\pi=1^+$ level at 2118 keV through a possible $M1$ transition of 863 keV. In addition, its observed decay patterns to the 1^+ and 2^+ states as well as the existence of a predicted 2^+ at similar energy are corroborating the proposed 2^+ assignment to this 1255 keV level. The 1932 keV state

likely has a $J^\pi=2_3^+$ configuration as it decays equally to the 1_1^+ ground state and to the 2_1^+ state. Moreover, the fact that it is fed directly from the 1_3^+ at 2.714 MeV and that a 2_3^+ is predicted at similar energy give further credit to this 2_3^+ spin assignment. We note that a $J^\pi=0^+$ assignment could not totally be excluded for two of the above arguments (presence of a predicted 0_1^+ at similar energy and feeding from the 1_3^+ state). However, in this hypothesis one would have expected a dominating decay of the 1932 keV excited state to the 1_1^+ ground state through an $M1$ transition and a much weaker decay to the 2_1^+ through an $E2$ transition. This is at variance with the observed equal decays to the 1_1^+ and 2_1^+ states, making the $J^\pi=2_3^+$ assignment of the 1932 keV more likely than $J^\pi=0_1^+$.

For all states predicted by the shell model calculations using the USDA interaction up to 2.2 MeV, except for the 0_2^+ and 4_1^+ states, candidates have been identified experimentally.

III. IN-BEAM γ -RAY SPECTROSCOPY

A. Experimental technique

In-beam γ -ray spectroscopy of the neutron-rich ^{28}Na isotope was performed in a second experiment at the NSCL facility at Michigan State University. As shown in Fig. 6, the ^{28}Na nuclei were produced in two-step fragmentation reactions. Firstly, a 140 MeV/u ^{48}Ca primary beam, delivered from the Coupled Cyclotron Facility, impinged on a 846 mg/cm² ^9Be primary target to produce a cocktail beam among which the ^{31}Mg and ^{32}Mg nuclei were chosen as secondary projectiles. They were selected in two independent settings using the A1900 fragment separator. An achromatic wedge of Al (300 mg/cm²) was inserted at the intermediate focal plane in order to purify the beams that were subsequently delivered to the experimental setup. Event-by-event identification was obtained from the time-of-flight between the A1900 (TOF start) and the S800 analysis line (TOF). At the S800 pivot point, the ^{31}Mg and ^{32}Mg nuclei impinged on a secondary ^9Be target (375 mg/cm²) at about 95 MeV/u. Reaction products, among them the desired ^{28}Na nuclei, were analyzed in the S800 spectrograph [41] and identified by their time-of-flights (between “TOF” and “TOF stop”) and energy losses measured in an ionization chamber (IC). This particle identification based on time-of-flight and energy loss is shown in Fig. 6 for the ^{31}Mg secondary beam setting. In total, about $7.7 \cdot 10^5$ γ - ^{28}Na coincidences were recorded in the two settings together. Their trajectories were tracked in the S800 spectrometer using two sets of Cathode Readout Drift Chambers (CRDC) that measured their position and angle values at the dispersive focal plane allowing the reconstruction of their four-momenta and position at the non-dispersive target location through ray-tracing. This event-by-event position and velocity ($\beta \simeq 0.41$) information is then used

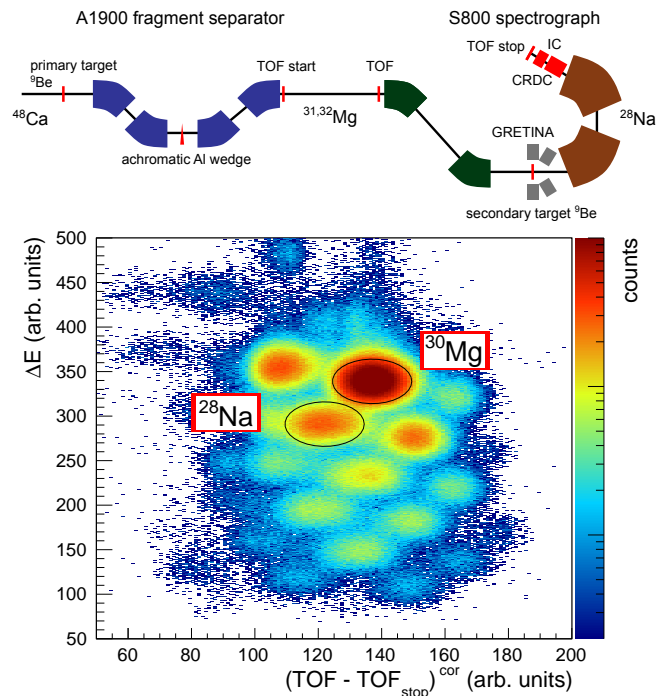


FIG. 6: (color on line) Top: Schematic view of the experimental set-up for the in-beam γ -ray spectroscopy of ^{28}Na produced in a double-step fragmentation reaction. Bottom: Event-by-event particle identification plot for reaction residues from the ^{31}Mg secondary beam. The plot shows the energy loss versus the time-of-flight measured between scintillators before and after the target, corrected for the different trajectories of the ions determined by means of the two sets of drift chambers. The circle indicates the ^{30}Mg one-neutron removal reaction residues as well as ^{28}Na .

to determine the emission angle of the γ -rays that is implemented in the Doppler-correction procedure. The target was surrounded by seven modules of the GRETINA array [34]. Four of them were placed at the most forward angles around 58° and three around 90° to detect γ rays induced by the in-flight de-excitation of the ^{28}Na nuclei. Each module of the GRETINA array consists in four HPGe segmented crystals. The γ -ray detection threshold has been lowered to about 50 keV in order to be able to observe the low-lying transition from the first excited state in ^{28}Na at 55 keV. The photopeak efficiency of the array has been determined using calibrated γ -ray sources. A good matching has been obtained between experimental and simulated efficiencies, the latter being obtained from a GEANT4 [42] modeling of the GRETINA setup [43]. This simulation was subsequently used to determine the full-energy peak efficiency for γ -rays emitted in-flight, which amounts to about 6 % at 1 MeV. The velocity vector and position of the ^{28}Na nuclei were used to apply an event-by-event Doppler correction to the γ -ray spectrum shown in Fig. 7. A γ -ray energy resolution (FWHM) of about 2% at 1 MeV was achieved. This resolution, that is limited by the velocity spread of the incoming beams, the energy loss in the target as well as

by the position resolution of GRETINA, is well reproduced by the GEANT4 simulation. Well-known energy transitions in neighboring nuclei (measured in the same experiment) could be reproduced within 3 keV. Transition energies may however be affected by an additional systematic uncertainty due to the unknown lifetime of decaying (and feeding states). Relative γ -ray intensities were obtained from a fit of the measured spectrum with simulated response functions of individual transitions, as shown in Fig. 7. The list of γ -ray energies and intensities observed in this experiment is given in Table II. The proposed spin parity assignments are based on the following discussion as well as on the β -decay study discussed above.

TABLE II: List of states, γ -ray energies and relative intensities observed in the in-beam experiment. The proposed spin parity assignments are based on the combination of the two experiments. A systematic uncertainty $\sigma(E)$ of about 3 keV should be considered for the proposed γ -ray energies derived from the in-beam work. Adopted energy values for the states, derived from the combination of the two experiments, are given in Fig. 10 with their corresponding error bars.

E_i (keV)	J_i^π	E_f (keV)	E_γ (keV)	I^{rel} (%) ^a
55	2^+	0	55	380(50)
688	$(3^+)^b$	55	633	100(2)
968	(4^+)	55	912 ^c	7(1)
		688	277	52(3)
1131	$(3^+)^b$	0	1131	1.9(6)
		55	1075	16.6(8)
1233	(2^-)	0	1233	1.9(6)
		55	1177	29(1)
		688	542	8.3(6)
1255	$(2^+)^b$	0	1255	15.7(8)
1353	(3^-)	55	1298	33(1)
1636	(4^-)	688	948	11.6(8)
		1233	403	16.7(7)
		1353	282	10(2)
1749	$(1^-, 2^-)$	55	1694	5.2(7)
1792	$(0^+, 1^-, 2^-)$	0	1792	6.9(9)
1929	$(2^+)^b$	0	1929	8.5(9) ^d
2121	1^+^b	55	2066	8.2(8) ^d
2378		0	2378	5.2(8) ^e
2493	(5^-)	965	1527	4(1)
		1636	858	14.8(8)
2605			2605	10(1) ^e
2650			2650	7(1) ^e
2874			2874	4(1) ^e
			1481	8.2(8) ^f
			489	5.7(6) ^e

^anormalized to the 633 keV transition

^bspin proposed from the β -decay experiment of ^{28}Ne

^cplacement based on energy difference

^dplacement based on β decay

^fplacement uncertain, potentially partially from ^{30}Mg

^eunplaced

The systematic uncertainty for the relative intensity of the 55 keV transition is particularly large because of the proximity of the detection threshold. Additionally, the

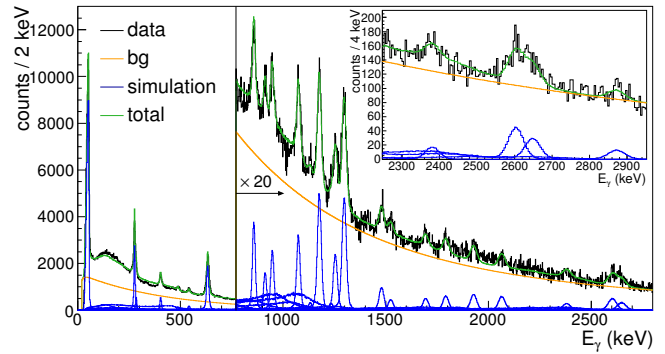


FIG. 7: (color on line) Doppler-reconstructed γ -ray energy spectrum obtained from the in-beam γ -decay spectroscopic study of ^{28}Na . The solid green line is the response obtained from the GEANT4 simulation of individual transitions (blue lines) and a continuous background (orange line) are considered. The inset shows the high energy part of the spectrum with in particular the doublet of transitions at 2605 and 2650 keV.

peak exhibits a low energy tail, making it partially not observable since some fraction of the intensity lies below the detection threshold. This tail is attributed to the fact that this state exhibits a relatively long lifetime. As a result, a significant fraction of its γ decay is occurring behind the target. For instance, the γ rays detected at 90° with respect to the target position and Doppler corrected as such, would in fact come from photons emitted beyond the target at backward angles with $\vartheta_{\text{emitt}} > 90^\circ$. The energy after Doppler correction is therefore lower than the transition energy leading to the asymmetric shape of the 55 keV γ peak with a tail towards low energies.

The lifetime of the 2^+ state has been simulated, and the resulting response function has been fitted to the shape of the experimental peak. This way, a lower limit for the lifetime of $\tau > 1$ ns is obtained. An additional constraint on the lifetime can be obtained from the fact that 100 % of the 633 keV γ -ray yield has to proceed through the 55 keV transition. Consistent yields in the 633-55 keV coincidence are obtained for simulated lifetimes of $\tau = 1.4(4)$ ns. Shell model calculations using the USDA effective interaction predict the 2^+ state at 182 keV. Using the shell model reduced transition probabilities, $B(E2)$ and $B(M1)$ values, for the decay to the ground state, and the experimental transition energy of 55 keV, a theoretical lifetime of $\tau_{\text{theo}} = 1.42$ ns is obtained.

Due to the high detection efficiency of the GRETINA array it was possible to construct γ - γ coincidence spectra by gating on several transitions. Fig. 8 shows the spectrum observed in coincidence with the 55 keV transition. This spectrum shows which of the observed γ transitions are directly or indirectly populating the first excited state at 55 keV.

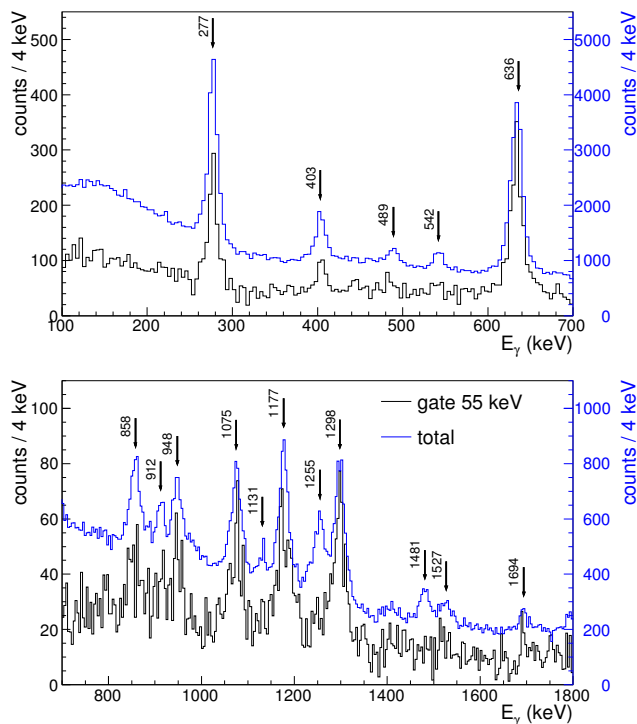


FIG. 8: (color on line) Doppler-reconstructed γ -ray energy spectrum gated on the 55 keV transition from the first excited state in ^{28}Na in two different energy ranges. The blue line (top spectrum in each panel) shows the total spectrum for comparison. While most of the transitions are observed in coincidence with the 55 keV γ ray, the transitions of 1255 and 1481 keV are for instance clearly missing in the γ -gated spectrum.

B. Level scheme of ^{28}Na

The level scheme of ^{28}Na as well as tentative spin assignments derived from this experiment are shown in Fig. 10. They are based on the relative intensities obtained from the singles γ -ray energy spectrum of Fig. 7, γ - γ coincidence spectra of Fig. 8 and 9 as well as γ branching ratios from Table II. Two almost overlapping γ transitions are present at 277 and 282 keV. The 633(3) keV γ -ray is compatible with the 636(1) keV γ -ray observed in the β -decay experiment. As the 564(1) keV γ -ray found in the β -decay experiment is not observed here, it is placed above the 636(1) keV transition. The 277(1) keV γ -transition is in coincidence with the 636 keV one. As the intensity of the latter is larger, it is placed below the 277 keV transition, establishing a new state at 968(3) keV as shown in Fig. 10.

A $J^\pi=4^+$ assignment is proposed for this level at 968(3) keV as it mainly decays by a 277 keV γ -ray to the previously assigned 3_1^+ at 691 keV, very weakly to the 55 keV 2_1^+ state and not to the ground state with $J^\pi=1^+$. Moreover, a 4^+ is predicted at similar energy by the shell model calculations, as shown in Fig. 10. With this newly

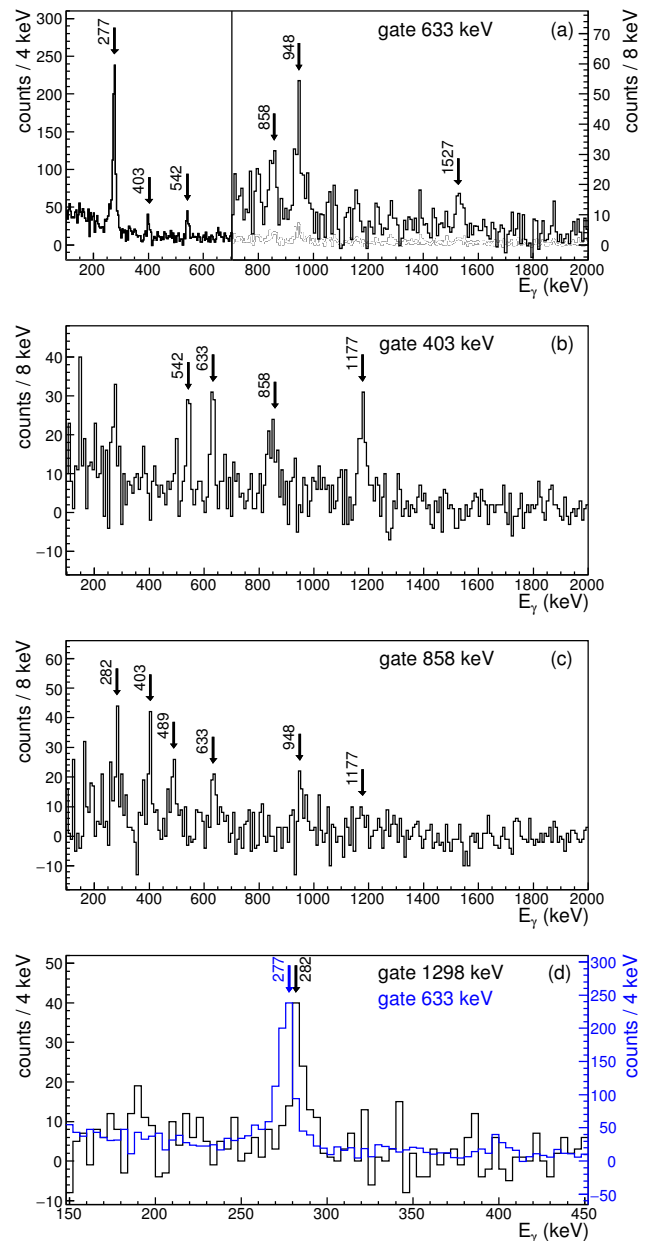


FIG. 9: (color on line) γ - γ coincidence spectra of ^{28}Na obtained during the in-beam experiment when gating on several γ -rays (from top to bottom 633, 403, 858 and (633,1298) keV).

proposed $J^\pi=4^+$ state, all positive parity states (but the $J^\pi=0^+$) that are predicted by the shell model calculations below 2.2 MeV are observed experimentally. It follows that the seven new states populated in the in-beam study of ^{28}Na and shown in the right part of Fig. 10 likely contain a candidate for $J^\pi=0^+$ as well as negative parity states arising from the neutron fp shells. Predicted energies of negative parity states were obtained using shell model calculations with the newly derived interaction WBA-M, whose detailed descriptions are given in Sect. IV C. The J assignment of these states is, as in

the β -decay study, based on the hierarchy of the transitions rates in their feeding (decay) from (to) identified states, this time considering that $E1$ transitions are much faster than $M2$ ones, as well as from the comparison to shell model calculations using the WBA-M interaction.

A $J^\pi=2^-$ assignment is proposed for the 1233 keV level from the fact that it decays to the $J^\pi=1^+$ ground state, to the $J^\pi=2_1^+$ state at 55 keV as well as to the $J^\pi=3_1^+$ state at 691 keV, but not to the $J^\pi=4_1^+$ state at 968 keV. This assignment is in accordance with the argument that $E1$ transitions are much faster than $M2$. The first 2^- state is predicted at 1552 keV by the shell model calculations, about 300 keV above the experimental value, as shown in Table. III.

A $J^\pi=3^-$ assignment is proposed to the 1353 keV level on the basis of its sole decay to the $J^\pi=2_1^+$ state through an $E1$ transition of 1298 keV. Its decay to the $J^\pi=4_1^+$ state through an $E1$ transition of 385 keV is not observed. This is likely due to the large energy difference between the two transitions (1298 and 385 keV) which largely favors the highest energy one by a factor of about 40, deduced from the $(1298/385)^3$ ratio expected between these two $E1$ transitions. A similar argumentation is proposed for the non observation of the decay to the $J^\pi=3_1^+$ state through an $E1$ of 662 keV, whose intensity is expected to be 8 times weaker than the 1298 keV branch. The first 3^- is predicted at 1715 keV, about 350 keV above the experimental value.

Owing to the fact that the 1792 keV state exclusively decays to the $J^\pi=1^+$ ground state, its spin assignment could be $J=0-2$. A larger J assignment would have led to the feeding of $J=3,4$ states. Moreover, as this state was not fed in the β -decay experiment, it is a likely candidate for a negative parity, i.e. either $J^\pi=1_1^-$ or 2_2^- that are both predicted by the WBA-M calculations, or $J^\pi=0^+$ that is predicted by the USDA calculations. A $J^\pi=0^-$ could not be rejected, even though its predicted energy is significantly higher than the present observation. Tentative spin $J^\pi=1^-$ and $J^\pi=2^-$ are also proposed for the state at 1749 keV based on its exclusive decays to $J^\pi=2_1^+$ state and the presence of predicted 1^- and 2^- about 400 keV above (see Table. III). This level could, however, neither be $J^\pi=0^+$ nor $J^\pi=0^-$ as it would have then preferentially decayed to the ground state through $M1$ or $E1$ transition rather to the $J^\pi=2_1^+$ with $E2$ or $M2$ transitions, respectively.

A new level is firmly established at 1636(2) keV from its observed three γ decay branches $282 + 1298 + 55$, $403 + 1177$ and $948 + 636 + 55$ keV. As this level decays to the $J^\pi=3_1^-$, $J^\pi=2_1^-$ and $J^\pi=3_1^+$ states and not to the $J=1,2$ positive parity states at lower energy, it is likely to have $J^\pi=4^-$. A positive parity state $J=4$ would not decay to the $J^\pi=2^-$ state as $M2$ transitions are strongly hindered and a higher spin value would also not decay to any of the lower energy $J=2$ states. The predicted 4^- state lies at 1888 keV, again about 300 keV higher in energy than the experimental value.

A $J^\pi=5^-$ level is proposed at 2493 keV from its 858

and 1527 keV γ branches to the previously assigned $J^\pi=4_1^-$ and $J^\pi=4_1^+$ states at 1636 and 968 keV, respectively, and from the non observation of its decay to lower spin states despite the larger γ -ray energies available for such transitions. The decay of the 2493 keV state to the $J^\pi=3_1^-$ state at 1353 keV through an $E2$ transition of 1140 keV is not observed. This branch is indeed expected to be much weaker than the $E1$ transition to the $J^\pi=4_1^+$ state that has, in addition to a smaller multipolarity, a largest available energy (1527 keV as compared to 1140 keV). The calculated 5^- level is at 2867 keV.

Other high energy γ -rays are observed at 2378, 2605, 2650 and 2874 keV. However, their placement in the level scheme is uncertain by 55 keV as there is not enough statistics to ensure that a coincidence with the 55 keV γ -ray is present or not. Finally, the 489 keV γ -ray could not be placed without ambiguity in the level scheme either.

IV. DISCUSSION

A. Positive parity states along the $N=17$ isotones

The level scheme of ^{28}Na shown in Fig. 10 has been obtained by combining the results from the β -decay (left part) and the in-beam γ spectroscopy (right part) experiments. The middle part of the spectrum displays transitions that are common to the two experiments. The two new levels with configurations $J^\pi = 3_1^+$ and 4_1^+ complete the quadruplet of $J^\pi=1^+-4^+$ states resulting from the proton-neutron $\pi d_{5/2} \otimes \nu d_{3/2}$ coupling in ^{28}Na . Added to the recently discovered $J^\pi=1^+-4^+$ states at low energy in the $N=17$ isotones of ^{26}F [28, 31, 32] and ^{30}Al [29], a systematics of their binding energies as a function of the proton-to-neutron binding energy asymmetry can be obtained and is compared to shell model calculations in Fig. 11. The energy difference between proton and neutron separation energies S_p-S_n ranges from 15 MeV in the close-to-drip-line nucleus ^{26}F to 7 MeV in ^{30}Al . For each nucleus the calculated binding energy of the ground state (using the USDA interaction) is taken as the reference value for Fig. 11.

The $J^\pi=1^+-4^+$ states in the ^{26}F nucleus can be described as a proton $\pi d_{5/2}$ coupled to a neutron in the $\nu d_{3/2}$ on top of a ^{24}O core nucleus. In this particle-particle coupling scheme, the multiplet of states in ^{26}F displays an upward pointing parabola in binding energy value as a function of J as seen in Fig. 11. In the present case the amplitude of the parabola scales to a first order with the strength of the residual interaction that splits the different components of the $J^\pi=1^+-4^+$ multiplet. With the exception of the tentatively assigned $J^\pi=3^+$ state that is unbound and therefore may need a specific treatment, the ordering of the states in ^{26}F is well reproduced by the USDA interaction but their calculated binding energies are too large by about 200 keV.

Even if the $J^\pi=1^+-4^+$ states proposed in [29] for ^{30}Al do not have a pure configuration, they can be viewed as

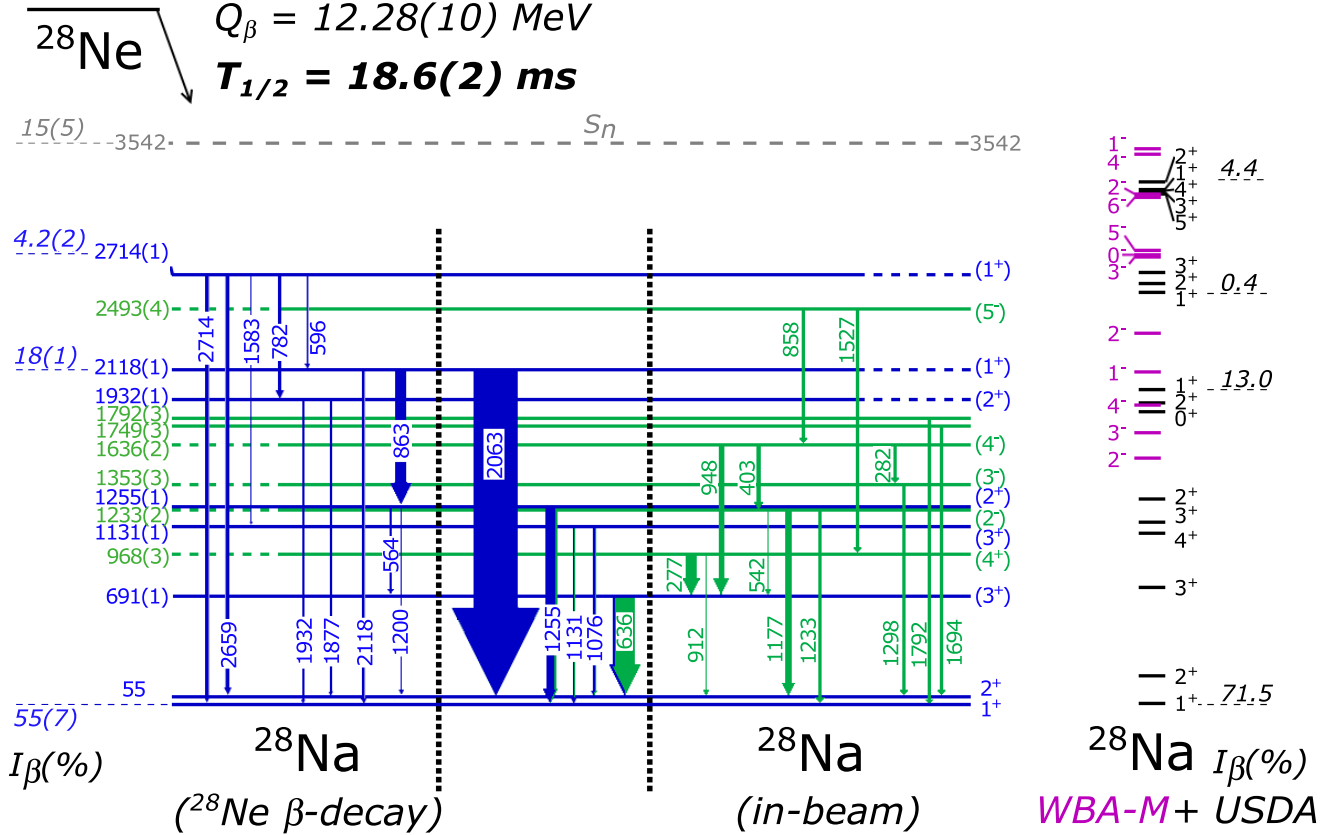


FIG. 10: (color on line) Experimental level scheme of ^{28}Na derived by adding information from the β -decay of ^{28}Ne (left, blue) and from the in-beam γ -ray spectroscopy of ^{28}Na (right, green). The thickness of the arrows represent the relative intensity of the transitions, normalized to the 2063 keV transition for the β -decay and to the 636 keV transition for the in-beam experiment, respectively. The middle part shows transitions, among which the 2063 keV one, that were observed in the two experimental studies. The very right part displays shell model predictions for negative parity states using the WBA-M interaction, together with positive parity states from the predictions of the USDA interaction. The energies and uncertainties of the levels are derived from the β -decay when possible (Table I), from the in-beam experiment (Table II), or from a combination of the two experiments otherwise. Tentative spin assignments for the levels at 1749 and 1792 keV are discussed in the text.

hole-particle coupling $(\pi d_{5/2})^{-1} \otimes \nu d_{3/2}$ states with respect to the full occupancy of the proton $d_{5/2}$ orbit. This leads to the downward pointing parabola as a function of J shown in Fig. 11. The amplitude and shape of the parabola is extremely well reproduced using the USDA interaction. However, the calculated absolute binding energies are this time smaller than the experimental values by about 300 keV.

The pattern of the binding energy of the $J^\pi=1^+-4^+$ states in ^{28}Na is intermediate between ^{26}F and ^{30}Al owing to the fact that the proton $d_{5/2}$ orbit is only half-filled. The spectrum of ^{28}Na is well reproduced by the USDA calculation. It is worth to notice here that a similar shift in binding energy is observed along the $N=17$ isotones when using the USDB [40] interaction. However the latter calculations proved to be less precise, predicting too small excitation energies of the $J^\pi=4^+$ state by about 600 keV in ^{26}F and 400 keV in ^{30}Al and a $J^\pi=2^+$

ground state of ^{28}Na instead of $J=1^+$.

Collecting all results along the $N=17$ isotonic chain, a systematic deviation between experimental and theoretical binding energies is observed: as compared to experimental values the ^{26}F is over bound, ^{28}Na is perfectly well reproduced, while ^{30}Al is under-bound. A total shift in energy of about 500 keV is found between these three isotones. Being a global shift in energy of the whole multiplet, this change in binding energy is likely caused by the monopole part of the $\pi d_{5/2} \otimes \nu d_{3/2}$ nuclear interaction rather than by multipoles. We propose three reasons that may explain this systematic deviation. First, on the experimental side, the atomic mass of ^{26}F derived in [44], that has been corrected in Ref. [28] to account for the possible contamination from the 4^+ isomeric state, may not be correct. This would account for the shift observed in ^{26}F but not in ^{30}Al . Second, the shell model calculations of [40] using the USDA or USDB interactions do

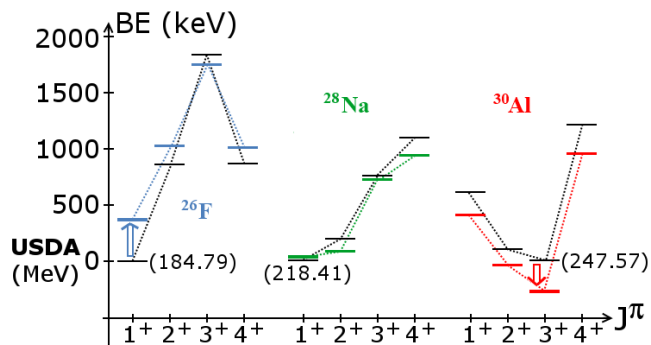


FIG. 11: (color on line) Comparison between the experimental binding energies of the $J^\pi = 1^+ - 4^+$ states in ^{30}Al [29, 46] (red), ^{28}Na [33, 46] and present work (green), and in ^{26}F [28, 31, 32, 44] (blue) and the USDA shell model predictions [40] (in black, labeled with the ground state binding energy value for each nucleus). Experimental binding energies in keV are referenced to the calculated ground state binding energy of each nucleus. Experimental binding energy uncertainties for the ^{30}Al , ^{28}Na and ^{26}F ground states are 14, 10 and about 130 keV, respectively.

not use an explicit isospin dependence of the Coulomb energy contribution to the binding energy of the nuclei as it probably should be done to account for the change of nuclear radii for a wide range of isotopes. This part is therefore taken only implicitly in the fitting procedure to determine the two-body matrix elements from the experimental data, a feature that can cause some bias in the calculation of the binding energies if the suitable data to constrain this isospin dependent part are not available experimentally or if they are not included in the fitting procedure. Third, the scaling law of the monopole interaction in $A^{-1/3}$ may not be appropriate, and more realistic interactions should be developed for nuclei spanning over a large proton-to-neutron binding energy asymmetry.

B. Negative parity states in the $N=17$ isotones

In the even- Z $N=17$ isotones, negative parity states $7/2^-$ and $3/2^-$ originating from the $0f_{7/2}$ and $1p_{3/2}$ neutron orbits have been populated at about 3 MeV through (d, p) reactions: in ^{33}S , the first $7/2^-$ and $3/2^-$ states lie at 2.934 and 3.220 MeV with C^2S values of 0.53 and 0.87, respectively [45]. In ^{31}Si , C^2S values for the first $7/2^-$ and $3/2^-$ at 3.133 and 3.535 MeV are 0.6 and 0.4, respectively [45]. In both cases, error bars of about 20% should be considered for the C^2S values, which, when close to unity, indicate a close-to-pure single particle configuration. Recently, negative parity states have been observed in ^{29}Mg and ^{27}Ne . Their excitation energies are much lower, and their ordering is reversed compared to ^{33}S and ^{31}Si , nuclei close to the valley of stability. States with $L=1$ and $L=3$ have been populated in ^{29}Mg at energies of 1096 and 1432 keV using the one neutron

knock-out reaction from ^{30}Mg [47]. Similar L assignments have been proposed in ^{27}Ne to the states at 0.765 ($3/2^-$, $L=1$) and 1.74 MeV ($7/2^-$, $L=3$) that are populated in the $^{26}\text{Ne}(d, p)^{27}\text{Ne}$ reaction with C^2S values of 0.64(33) and 0.35(10), respectively [25].

Qualitatively, as protons are removed from the $0d_{5/2}$ orbit from ^{31}Si , the excitation energy of the two negative parity states $7/2^-$ and $3/2^-$ is decreasing relatively to the $3/2^+$ ground state, and their ordering is reversed around $Z=12$. It is derived that the $N=20$ gap between the neutron $0d_{3/2}$ and $0f_{7/2}$ is collapsing and the order of the neutron $0f_{7/2}$ and $1p_{3/2}$ orbitals, which form the traditional $N=28$ gap, is reversed. These features have been qualitatively attributed in Ref. [16] to the hierarchy of the proton nuclear forces.

In the odd-odd nuclei such as ^{30}Al or ^{28}Na , multiplet of negative parity states $J^\pi=1^- - 4^-$ and $J^\pi=1^- - 6^-$ are expected to be formed by the proton-neutron coupling $0d_{5/2} \otimes 1p_{3/2}$ and $0d_{5/2} \otimes 0f_{7/2}$, respectively. The lowest energy negative parity state in ^{30}Al observed in [29, 30], and proposed as a 4^- candidate, lies at about 2.3 MeV. While states of lower spin value may have not been observed in $^{30}\text{Al}_{13}$ from these works, the presently proposed negative parity states down to 1.233 MeV in $^{28}\text{Na}_{11}$ suggests a decrease in energy of the intruder orbits between $Z=13$ and $Z=11$. The present observation of tentatively assigned negative parity states $J=1^-, 2^-, 3^-$ and 4^- in ^{28}Na at low energies of 1749 (or 1792), 1233, 1353 and 1636 keV, respectively, is in accordance with the presence of the neutron $1p_{3/2}$ orbit at relatively low energy at $Z=10$ [25]. Contingent on future confirmation, these $J=1-4$ negative parity states are systematically more bound than theoretically predicted (by about 300 keV, see Table III). This would hint at a possibly stronger proton-neutron $0d_{5/2} - 1p_{3/2}$ interaction than calculated. The tentatively assigned $J^\pi=5^-$ state at 2493 keV (calculated at 2867 keV) is in accordance with the presence of the $0f_{7/2}$ orbit about 1 MeV above the $1p_{3/2}$ orbit, as proposed in ^{27}Ne [25].

C. Evolution of nuclear structure towards the drip-line

In order to understand the evolution of the neutron $1p_{3/2}$ orbit and the $N=20$ gap towards the neutron drip line, configuration-interaction (CI) calculations were carried out with a Hamiltonian called WBA. It is the same as the WBP Hamiltonian from [48], but the older USD sd-shell Hamiltonian [49] part was replaced by the more recent USDA Hamiltonian [40] that was used in the previous section to calculate the energy of positive-parity states. The required basis to model the $N=17$ isotones is the full $(1s0d)$ for positive parity states with a core of ^{16}O . Moreover, it allows for one neutron to be excited to the $(1p0f)$ valence space for negative parity states. While this basis can be used for low-lying negative-parity states in ^{25}O , ^{26}F or ^{27}Ne , the dimension of the calculation is

TABLE III: Excitation energies of some low-lying negative-parity states obtained with the WBA-M Hamiltonian in the $N=17$ isotones.

Nucleus	J^π	E_x (MeV)
^{25}O	$3/2^-$	0.493
	$1/2^-$	1.898
	$7/2^-$	2.611
^{26}F	4^-	1.339
	2^-	1.384
	1^-	1.952
	3^-	2.485
^{27}Ne	$3/2^-$	0.825
	$7/2^-$	1.710
	$1/2^-$	1.834
^{28}Na	2^-	1.552
	3^-	1.715
	4^-	1.888
	1^-	2.100
	2^-	2.341
	3^-	2.821
	0^-	2.836
	5^-	2.867

at the limit for ^{28}Na and too large for ^{29}Mg and ^{31}Si . Such calculations might be possible in the future.

The WBA interaction was used to calculate the energies of negative-parity states in ^{27}Ne . As they were too high by 0.4 MeV, the single-particle energies of the $1p-0f$ shell orbitals have been modified by 0.4 MeV, leading to the WBA-M interaction. The energies of the positive parity states obtained with this interaction are those calculated with the USDA interaction. With this WBA-M interaction, the $3/2^-$ state in ^{27}Ne at 765 keV [25–27] is calculated at 825 keV, while the $7/2^-$ at 1.74 MeV [25] is calculated at 1.71 MeV. Excitation energies of low-lying negative parity states are given in Table III for the $N=17$ isotones that the model can handle. In ^{28}Na negative parity states are predicted at low excitation energies, in the same energy range where candidates have been identified experimentally in this work. The wave functions of the first $J^\pi=1^- -4^-$ are composed by 60-75% of a neutron in the $1p_{3/2}$ and by 20-30% of a neutron in the $0f_{7/2}$ orbital, the remaining weak fraction being distributed in the neutron $1p_{1/2}$ and $0f_{5/2}$ orbitals. All calculated negative parity states in ^{26}F lie above the neutron emission threshold of $S_n = 1.070(62)$ MeV, a feature that agrees with the observation of only two bound excited states of positive parity in this nucleus [28]. In ^{25}O , the $3/2^-$ is expected to lie only 493 keV above the $3/2^+$ resonance [22]. The three negative-parity states $3/2^-$, $7/2^-$ and $1/2^-$ in ^{25}O have large $^{24}\text{O}+n$ spectroscopic factors. With the proximity in energy between the $3/2^+$ and $3/2^-$ states in ^{25}O , ^{26}O likely contains a significant amount of negative parity contribution in its ground and first excited states.

The reliability of this extrapolation far from stability would certainly benefit from the confirmation of spin as-

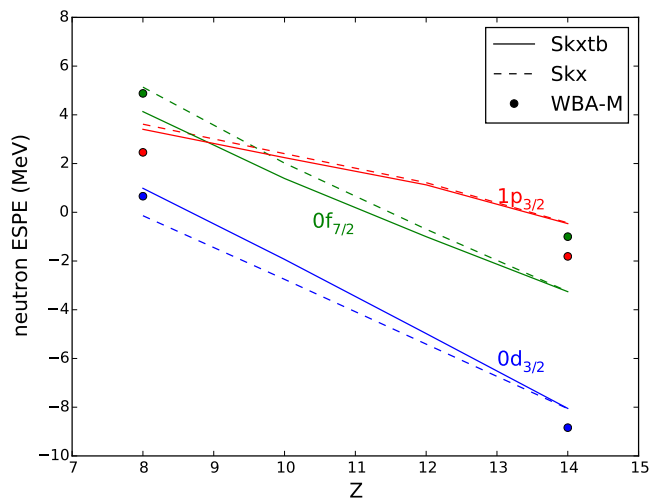


FIG. 12: (color on line) Effective single-particle energies of the $0d_{3/2}$, $0f_{7/2}$ and $1p_{3/2}$ orbits calculated for nuclei with an $N=16$ core using two Skyrme functionals that implements tensor forces (full line, Skxtb) or not (dashed line, Skx). The down bending of the unbound $1p_{3/2}$ orbital observed when reaching the drip line is due to the halo like structure of the nuclei. The results for the configuration-interaction (CI) model with the WBA-M interaction are shown for comparison with the filled circles at $Z=8$ and $Z=14$.

signments of negative parity states in ^{28}Na , the possibility to model higher Z isotones in this large valence space, and the observation of negative parity states in ^{26}F in the future.

The present shell evolution towards the neutron drip line, shown with filled circles in Fig. 12 at $Z=14$ and $Z=8$, is made in an Harmonic Oscillator basis in which bound and unbound states are treated on the same footing. Therefore we looked at trends of Effective Single Particle Energies (ESPE) in the framework of Energy Density Functional (EDF) calculations that do not use a Harmonic Oscillator basis. The single-particle energies $0d_{3/2}$, $0f_{7/2}$ and $1p_{3/2}$ orbits obtained with the Skx [50] and Skxtb [51] Skyrme functionals are shown with lines of different colors in Fig. 12 for a $N=16$ core as a function of proton number. This figure is similar to Fig. 1, the major changes consisting here in the down bending of the neutron $1p_{3/2}$ orbital when reaching the drip line and a weaker reduction of the $N=20$ gap (between the neutron $0d_{3/2}$ and $0f_{7/2}$ orbits). This non linearity in the ESPE of the $1p_{3/2}$ orbital is due to its halo-like nature that is reducing the effective monopole interactions there. The weak-binding effect in the single-particle energies for the low- l orbitals for light nuclei has been discussed by Hamamoto [52] (see Figs. 3 and 4 in [52]). It is the same mechanism that reduces the neutron $1s_{1/2}-0d_{5/2}$ gap for the region of $Z=2-8$ as shown by the EDF calculations in Fig. 1 of [53], and more recently by calculations with a Woods-Saxon potential [54]. Basically the binding energy of the low- l orbitals is more significantly affected by

the proximity to the continuum as they encounter a much smaller centrifugal barrier than higher- l orbits.

Fig. 12 also shows the results of two different EDF calculations. Skx does not contain a tensor interaction, while for Skxtb a tensor interaction has been added that describes the trends of single-particle energies in heavier nuclei [51]. The ESPE for Skx and Skxtb are the same for $Z=14$ since the Skxtb tensor interaction for protons and neutrons cancel for the doubly jj closed shells in ^{28}Si . From $Z=14$ to $Z=8$ protons are removed from the proton $0d_{5/2}$ orbital. The tensor interaction between the $0d_{5/2}$ protons and the $0d_{3/2}$ neutrons increases to its maximum for $Z=8$. This increases the ESPE of the neutron $0d_{3/2}$ orbital and makes it unbound at $Z=8$. It also decreases the ESPE of the neutron $0f_{7/2}$ orbital. Thus, in the EDF model the $N=20$ shell gap at $Z=8$ is reduced due to a combination of the tensor-interaction effect for the neutron $0d_{3/2}-0f_{7/2}$ ESPE spacing and the weak binding effect for the neutron $0d_{3/2}-1p_{3/2}$ ESPE spacing.

The ESPE have been evaluated using the WBA-M interaction by restricting the neutron core to have a $(0d_{5/2})^6, (1s_{1/2})^2$ neutron configuration. They are shown in Fig. 12 at $Z=8$ and $Z=14$ and compared to EDF results.

V. SUMMARY

The spectroscopy of ^{28}Na has been investigated by means of the β -decay of ^{28}Ne at GANIL/LISE and the in-beam γ -ray spectroscopy through the fragmentation of $^{31,32}\text{Mg}$ beams at the NSCL/S800. New positive parity states with $J^\pi=3^+$ and 4^+ are proposed at 691 and 968 keV, respectively, while new negative parity states are proposed at 1233, 1353, 1636 and 2493 keV with likely spin assignments $J^\pi=2^-$, $J=3^-$, 4^- and 5^- , respectively. Other negative parity states are tentatively proposed at 1749 and 1792 keV, the spin and parity assignments of which are more uncertain. Using these complementary methods all components belonging to the multiplet of states $J^\pi=1^+-4^+$ arising from the proton-neutron $0d_{5/2}-0d_{3/2}$ coupling have been discovered. With the recent studies of the same multiplet of states in the ^{26}F and ^{30}Al isotones, the evolution of the binding energy of the $J^\pi=1^+-4^+$ multiplet for the $N=17$ isotones, that contain a single neutron in the $0d_{3/2}$ orbit, has been determined. The binding energy evolution as a function of J is changing from an upward to a downward pointing parabola as protons $0d_{5/2}$ are added between ^{26}F (one particle in $0d_{5/2}$) and ^{30}Al (one hole in $0d_{5/2}$). This trend nicely follows the proton-neutron particle-particle to hole-particle coupling scheme for odd-odd nuclei, indicating that the $N=16$ and $Z=14$ subshells are closed enough to allow this description. This picture has then been compared to shell model predictions using the USDA interaction. While the relative energies of the $J^\pi=1^+-4^+$ states are well reproduced with the USDA interaction in the $N=17$ isotones, a progressive shift in binding energy of the whole multi-

plet (that amounts to about 500 keV in total) is observed when moving from the valley of stability in ^{30}Al to the drip line in ^{26}F . The origin of this shift may arise from a change in the proton-neutron $0d_{5/2}-0d_{3/2}$ effective interaction when exploring large proton to neutron binding energy asymmetry. Other possible reasons are proposed as well, such as a possibly wrong mass measurement of the ^{26}F , in which a β -decay isomer was recently discovered, or/and by the lack of an explicit treatment of the isospin dependence of the Coulomb energy contribution to the binding energy of the nuclei.

The tentative presence of a multiplet of negative parity states $J^\pi=1^-4^-$ around 1.5 MeV, likely arising from the $\pi d_{5/2}-\nu p_{3/2}$ coupling, as well as a tentative observation of a $J=5^-$ state around 2.5 MeV, likely arising from the $\pi d_{5/2}-\nu f_{7/2}$ coupling, suggest the collapse of the $N=20$ gap and the inversion between the neutron $f_{7/2}$ and $p_{3/2}$ levels when removing protons from the $d_{5/2}$ orbital toward the drip line. States of similar parity are predicted by shell model calculations using the WBA-M interaction. They are however globally less bound than experiment by about 300 keV, a feature that may be due to a slightly wrong determination of the effective interactions involved. These shell evolutions have been discussed in the framework of Shell Model and EDF calculations, leading to the conclusions that no bound negative parity state would be present in ^{26}F and that the $3/2^+$ ground state and $3/2^-$ first excited states would be separated by only about 500 keV in ^{25}O .

On the experimental side, it is important to confirm in the future the spin and parity assignments of the proposed negative parity states in ^{28}Na using for instance the $^{27}\text{Na}(d,p)^{28}\text{Na}$ reaction. On the theoretical side, the evolution of the neutron $sd-pf$ orbits from the valley of stability to the drip-line is not yet satisfactorily treated by shell model calculations due to the possibly incorrect effective interactions, to the technical difficulty to handle high dimension calculations as well as to the non-implementation of continuum effects. This combined experimental and theoretical study of shell evolution along a chain of isotones from the stability to the drip-line is a pioneering and benchmarking work for future studies in other regions of the chart of nuclides.

VI. ACKNOWLEDGMENTS

This work is supported by the National Science Foundation (NSF) under Grant Nos. PHY-1102511, PHY-1306297 and PHY-1404442, by the OTKA contract K100835, the German BMBF (Grant No. 05P12RDFN8) and HIC for FAIR. GRETINA was funded by the US DOE - Office of Science. Operation of the array at NSCL is supported by NSF under Cooperative Agreement PHY-1102511 (NSCL) and DOE under grant DE-AC02-05CH11231 (LBNL). F. Nowacki is acknowledged for fruitful discussions.

-
- [1] C. Thibault et al., Phys. Rev. C **12**, 644 (1975).
[2] G. Hubert et al., Phys. Rev. C **18**, 2342 (1978).
[3] C. Détraz et al., Phys. Rev. C **19**, 164 (1979).
[4] D. Guillemaud-Mueller et al., Nucl. Phys. A **426**, 37 (1984).
[5] T. Motobayashi et al., Phys. Lett. B **346**, 9 (1995); H. Iwasaki et al., Phys. Lett. B **522**, 9 (2001); B. V. Pritychenko et al., Phys. Rev. C **63**, 011305(R) (2000); J.A. Church et al., Phys. Rev. C **72**, 054320 (2005); Y. Yanagisawa et al., Phys. Lett. B **566**, 84 (2003).
[6] R. Neugart, G. Neyens, Lect. Notes Phys. **700** 135 (2006); M. Kowalska, et al., Phys. Rev. C **77**, 034307 (2008); G. Neyens, et al., Phys. Rev. Lett. **94**, 022501 (2005); D. Yordanov, et al., Phys. Rev. Lett. **99**, 212501(2007).
[7] J. Terry et al., Phys. Rev. C **77**, 014316 (2008).
[8] F. Rotaru et al., Phys. Rev. Lett. **109**, 092503 (2012).
[9] K. Wimmer et al., Phys. Rev. Lett. **105**, 252501 (2010).
[10] O. Sorlin and M.G. Porquet, Prog. Part. Nucl. Phys. **61**, 602 (2008).
[11] X. Campi et al., Nucl. Phys. A **251**, 193 (1975).
[12] A. Poves and J. Retamosa, Phys. Lett. B **184**, 311 (1987).
[13] E.K. Warburton, J. A. Becker and B. A. Brown, Phys. Rev. C **41**, 1147 (1990).
[14] Y. Utsuno et al., Phys. Rev. C **60**, 054315 (1999).
[15] T. Otsuka et al., Phys. Rev. Lett. **95**, 232502 (2005).
[16] O. Sorlin, proceedings of the INPC 2013 conference, Florence, Italy 2013, EPJ Web of Conferences **66**, 01016 (2014).
[17] P.G. Thirolf et al., Phys. Lett. B **485**, 16 (2000).
[18] M. Stanoiu et al., Phys. Rev. C **69**, 034312 (2004).
[19] A. Ozawa et al., Phys. Rev. Lett. **84**, 5493 (2000).
[20] E. Becheva et al. Phys. Rev. Lett. **96**, 012501 (2006)
[21] C. R. Hoffman et al., Phys. Lett. B **672**, 17 (2009).
[22] C. R. Hoffman et al., Phys. Rev. Lett. **100**, 152502 (2008).
[23] K. Tshoo et al., Phys. Rev. Lett. **109** 022501 (2012).
[24] W.N. Catford et al., Phys. Rev. Lett. **104** 192501 (2010).
[25] S. M. Brown et al., Phys. Rev. C **85**, 011302 (R) (2012).
[26] A. Obertelli, et al., Phys. Lett. B **633**, 33 (2006).
[27] J. R. Terry, et al., Phys. Lett. B **640**, 86 (2006).
[28] A. Lepailleur et al., Phys. Rev. Lett. **110**, 082502 (2013).
[29] D. Steppenbeck et al., Nucl. Phys. A **847**, 149 (2010).
[30] T. A. Hinnners et al., Phys. Rev. C **77**, 034305 (2008).
[31] M. Stanoiu et al., Phys. Rev. C **85**, 017303 (2012).
[32] N. Frank et al., Phys. Rev. C **84**, 037302 (2011).
[33] V. Tripathi et al., Phys. Rev. Lett. **94**, 162501 (2005); Phys. Rev. C **73**, 054303 (2006).
[34] S. Paschalis et al., Nucl. Instr. and Meth. in Phys. Res. A **709**, 44 (2013).
[35] R. Anne and A.C. Mueller, Nucl. Inst. Meth. B **70**, 276 (1999).
[36] J. Simpson et al., Acta Phys. Hung., New Series, Heavy Ion Physics **11**, 159 (2000).
[37] D. Guillemaud-Mueller et al., Nucl. Inst. Meth. A **426**, 37 (1984).
[38] K. Kura et al. Phys. Rev. C **85**, 034310 (2012).
[39] L. Weissman et al., Phys. Rev. C **70**, 057306 (2004).
[40] B.A. Brown and W.A. Richter, Phys. Rev. C **74**, 034315 (2006).
[41] D. Bazin et al., Nucl. Instr. and Meth. in Phys. Res. B **204**, 629 (2003).
[42] S. Agostinelli et al., Nucl. Inst. Meth. A **506**, 250 (2003).
[43] L. A. Riley, UCGretina, unpublished.
[44] B. Jurado et al., Phys. Lett. B. **649** 43 (2007).
[45] Evaluated Nuclear Structure Data File (ENSDF), Brookhaven National Laboratory, <http://www.nndc.bnl.gov/ensdf/>.
[46] M. Wang et al., Chinese. Physics C **36**, 1603 (2012).
[47] J. R. Terry et al., Phys. Rev. C **77**, 014316 (2008).
[48] E. K. Warburton and B. A. Brown, Phys. Rev. C **46**, 923 (1992).
[49] B. A. Brown and B. H. Wildenthal, Ann. Rev. of Nucl. Part. Sci. **38**, 29 (1988).
[50] B. A. Brown, Phys. Rev. C **58**, 220 (1998).
[51] B. A. Brown, T. Duguet, T. Otsuka, D. Abe and T. Suzuki, Phys. Rev. C **74**, 061303(R) (2006).
[52] I. Hamamoto, Phys. Rev. C **76**, 054319 (2007).
[53] H. Sagawa, B. A. Brown and H. Esbensen, Phys. Lett. B **309** 1, (1993).
[54] C. R. Hoffman, B. P. Kay and J. P. Schiffer, Phys. Rev. C **89**, 061305(R) (2014).